RESEARCH LETTER

Key Points:
- First direct evidence of equatorial plane exhausts at 22 of 42 compressed KH-related current sheets
- MMS observed an equal probability of inward and outward directed exhausts along the magnetopause
- MMS observed asymmetric Hall magnetic and electric fields consistent with a strong guide-field and a weak density asymmetry

Supporting Information:
- Supporting Information S1
- Figure S1
- Figure S2

Correspondence to:
S. Eriksson,
eriksson@lasp.colorado.edu

Magnetospheric Multiscale observations of magnetic reconnection associated with Kelvin-Helmholtz waves

S. Eriksson[1], B. Lavraud[2,3], F. D. Wilder[1], J. E. Stawarz[1], B. L. Giles[4], J. L. Burch[5], W. Baumjohann[6], R. E. Ergun[1], P.-A. Lindqvist[7], W. Magnes[6], C. J. Pollock[4], C. T. Russell[8], Y. Saito[9], R. J. Strangeway[8], R. B. Torbert[10], D. J. Gershman[4], Yu. V. Khotyaintsev[11], J. C. Dorelli[4], S. J. Schwartz[1,12], L. Avanov[4], E. Grimes[8], Y. Vernisse[2,3], A. P. Sturner[1], T. D. Phan[13], G. T. Marklund[7], T. E. Moore[4], W. R. Paterson[4], and K. A. Goodrich[1]

[1]Laboratory for Atmospheric and Space Physics, University of Colorado Boulder, Boulder, Colorado, USA, [2]Institut de Recherche en Astrophysique et Planétologie, Université de Toulouse, Toulouse, France, [3]Centre National de la Recherche Scientifique, UMR 5277, Toulouse, France, [4]NASA Goddard Space Flight Center, Greenbelt, Maryland, USA, [5]Southwest Research Institute, San Antonio, Texas, USA, [6]Space Research Institute, Austrian Academy of Sciences, Graz, Austria, [7]Royal Institute of Technology, Stockholm, Sweden, [8]Institute of Geophysics and Planetary Physics, and Department of Earth, Planetary, and Space Sciences, University of California, Los Angeles, California, USA, [9]Institute for Space and Astronautical Science, Sagamihara, Japan, [10]Physics Department and Space Science Center, University of New Hampshire, Durham, New Hampshire, USA, [11]Swedish Institute of Space Physics, Uppsala, Sweden, [12]Blackett Laboratory, Imperial College London, London, UK, [13]Space Sciences Laboratory, University of California, Berkeley, California, USA

Abstract The four Magnetospheric Multiscale (MMS) spacecraft recorded the first direct evidence of reconnection exhausts associated with Kelvin-Helmholtz (KH) waves at the duskside magnetopause on 8 September 2015 which allows for local mass and energy transport across the flank magnetopause. Pressure anisotropy-weighted Walén analyses confirmed in-plane exhausts across 22 of 42 KH-related trailing magnetopause current sheets (CSs). Twenty-one jets were observed by all spacecraft, with small variations in ion velocity, along the same sunward or antisunward direction with nearly equal probability. One exhaust was only observed by the MMS-1,2 pair, while MMS-3,4 traversed a narrow CS (1.5 ion inertial length) in the vicinity of an electron diffusion region. The exhausts were locally 2-D planar in nature as MMS-1,2 observed almost identical signatures separated along the guide-field. Asymmetric magnetic and electric Hall fields are reported in agreement with a strong guide-field and a weak plasma density asymmetry across the magnetopause CS.

1. Introduction

The Earth's magnetopause flanks constantly experience a variable flow shear between stagnant or weakly drifting plasma in the magnetosphere and a strong and variable antisunward plasma flow in the adjacent magnetosheath due to the shocked solar wind. Certain conditions of plasma flow shear and directions of the ambient magnetic field (**B**) across the low-latitude magnetopause current sheet (CS) allow the Kelvin-Helmholtz (KH) instability [e.g., *Chandrasekhar*, 1961; *Miura and Pritchett*, 1982] to grow and form magnetopause surface waves that propagate in the antisunward direction of the magnetosheath flow [e.g., *Kivelson and Chen*, 1995]. The wave amplitude is expected to grow and generate rolled-up flow vortices in the nonlinear phase of its evolution along the flank [e.g., *Fairfield et al.*, 2000; *Hasegawa et al.*, 2004, 2006; *Foullon et al.*, 2008; *Nakamura et al.*, 2013]. The KH instability can readily grow if **B** is perpendicular to the KH wave vector **k** on either side of the magnetopause. This is expected to occur, as corroborated by observations, if the interplanetary magnetic field (IMF) has a significant component along the Z_{GSE} axis [e.g., *Kokubun et al.*, 1994].

A finite component of **B** along the flow shear direction will exert a stabilizing force and lower the KH growth. This in-plane B_L may be wrapped up within evolving KH vortices, where it may be further compressed and form intense CS which may become sites of magnetic reconnection [e.g., *Nykyri and Otto*, 2001; *Nakamura and Fujimoto*, 2005; *Nykyri et al.*, 2006]. A magnetic field with a dominant out-of-plane B_M component and oppositely directed in-plane B_L components across the magnetopause may also form intense CS along the sunward facing, trailing edges of KH waves where the magnetosheath flow acts to compress the magnetopause [e.g., *Pu et al.*, 1990; *Knoll and Chacón*, 2002; *Nakamura et al.*, 2008, 2013]. They form at an early linear phase of the KH evolution and persist into the nonlinear stage of rolled-up KH vortices [*Nakamura et al.*,
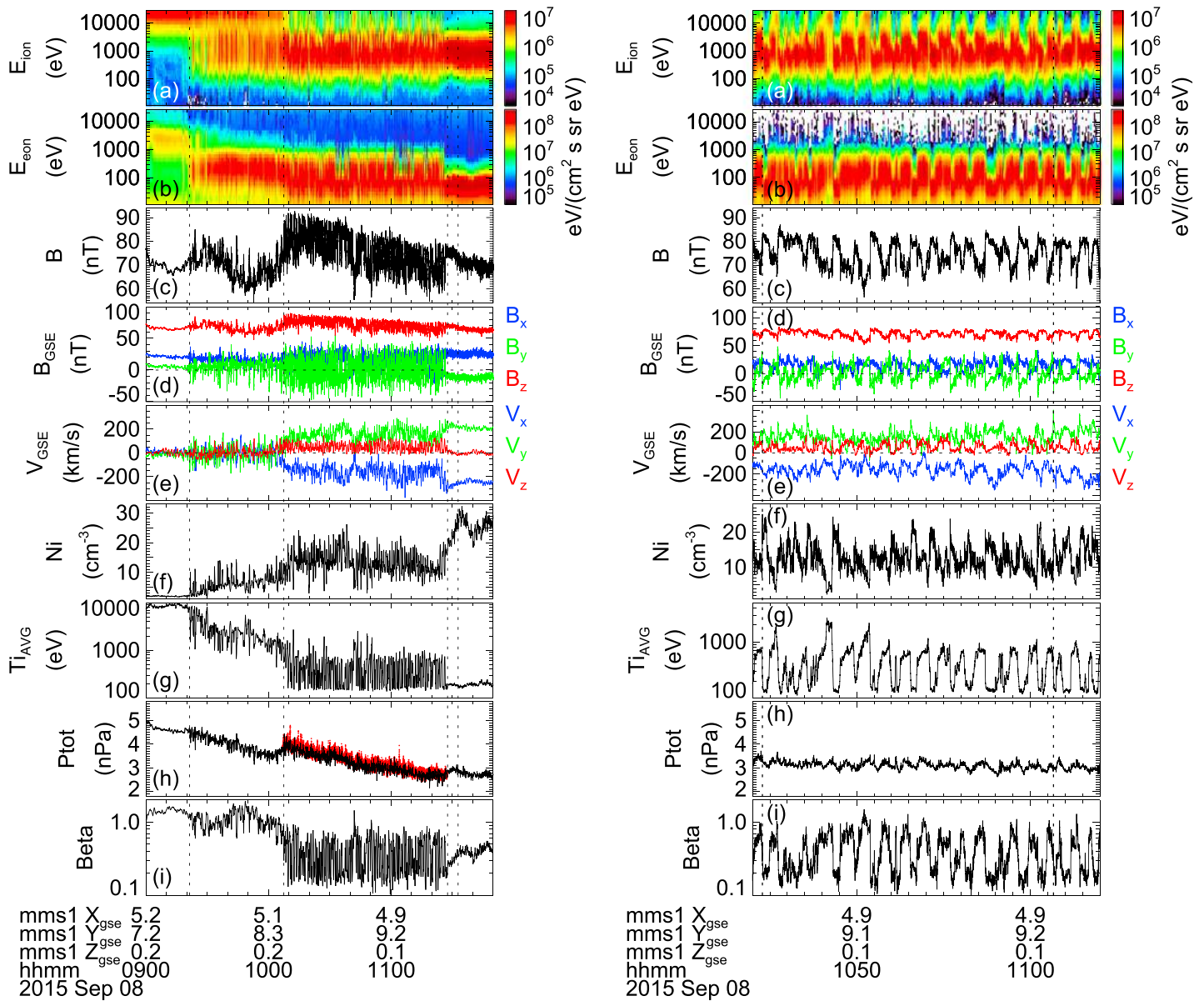
Figure 1. MMS-1 observations are shown 09:00–11:50 UT (left, fast survey) and 10:44–11:04 UT (right, burst mode) on 8 September 2015. The figure displays omni-directional energy-time spectrograms for (a) ions and (b) electrons, (c) **B** magnitude, (d) GSE components of **B**, (e) GSE components of the ion velocity, (f) ion plasma number density (N_i), (g) average ion temperature (T_{iAVG}), (h) sum of the magnetic pressure $P_b = B^2/2\mu_0$, ion plasma pressure $P_i = N_i k_B T_{iAVG}$, and electron plasma pressure $P_e = N_e k_B T_{eAVG}$ (black: fast survey; red: burst), and (i) total plasma β. Vertical dashed lines (Figure 1, right) highlight the two CS reported in detail in this letter.

2013]. *Hasegawa et al.* [2009] reported the first indication of an in-plane magnetic reconnection exhaust from an **E** × **B** observation across a ~240 km wide KH-related trailing CS behind the duskside terminator. However, the 3 s duration of this CS was too brief to confirm the presence of a plasma exhaust with Cluster measurements.

The Magnetospheric Multiscale (MMS) mission [*Burch et al.*, 2015] with its unprecedented high-resolution ion (150 ms) and electron (30 ms) measurements [*Pollock et al.*, 2016], magnetic fields [*Russell et al.*, 2014], and electric fields [*Torbert et al.*, 2014; *Ergun et al.*, 2014; *Lindqvist et al.*, 2014] allows for the first in-depth analysis of intense CS forming at the trailing edges of KH-related surface waves in a strong guide-magnetic field, in order to explore whether they support magnetic reconnection. In this letter we provide the first direct evidence in agreement with KH-related reconnection exhausts at narrow, low-field shear CS with durations as low as 1.2 s across a duskside magnetopause on 8 September 2015. We also report evidence for the

presence of highly asymmetric Hall magnetic and electric fields [e.g., *Sonnerup*, 1979; *Terasawa*, 1983; *Pritchett*, 2001; *Drake et al.*, 2009; *Eastwood et al.*, 2010] consistent with a strong guide-field and a weak plasma density asymmetry across the magnetopause CS.

2. Overview of MMS Observations on 8 September 2015

The MMS mission was launched on 12 March 2015 into a 12 R_E apogee elliptical orbit in the equatorial plane to explore where magnetic reconnection occurs in the Earth's magnetosphere and what factors influence this universal plasma physics process. The initial phase of the mission began on 1 September 2015 [*Fuselier et al.*, 2014] to target the dayside magnetopause with short periods of burst data collected at selected magnetopause CS by a team of MMS Scientists-In-The-Loop (SITL). This letter examines a flank magnetopause period when an interplanetary flux rope encountered the Earth on 7–9 September 2015 with a core IMF $\mathbf{B}_{GSE} = (13.7 \pm 0.9, -2.7 \pm 1.6, 15.6 \pm 0.6)$ nT. The MMS satellites were moving across the low-latitude boundary layer and into the magnetosheath at approximately $(x,y,z)_{GSE} = (4.9, 9.2, 0.1)$ R_E or 15.7 h magnetic local time (MLT), with an interspacecraft tetrahedron separation of 150–185 km when the magnetosphere was immersed within this flux rope.

Figure 1 (left) shows MMS-1 fast survey observations between 09:00 and 11:50 UT on 8 September 2015. Energy-time spectrograms of ions and electrons show that MMS was inside the magnetosphere proper until 09:21:24 UT (first vertical dotted line) characterized by a low plasma density and high ion temperature, slow average ion velocity, and a geomagnetic field $\mathbf{B}_{GSE} = (20,5,65)$ nT. This was followed by a 2 h long interval of boundary layer plasma. Significant variations were observed in the ion temperature and $\mathbf{B}$ during the last ~80 min of this period between 10:07:30 UT (second vertical line) and 11:27:40 UT (third vertical line) when MMS exited into the cold, dense magnetosheath plasma. The first 5 min of the magnetosheath is consistent with a low-β plasma depletion layer (PDL) [e.g., *Wang et al.*, 2003] with a weakly compressed northward $\mathbf{B}_{GSE} = (27, -8, 70)$ nT and a lower plasma density coincident with a faster $\mathbf{V}_{GSE} = (-278, 223, 10)$ km/s flow than what is observed after 11:32:50 UT (fourth vertical line) when the flow slowed down to a steady $\mathbf{V}_{GSE} = (-251, 214, -12)$ km/s with a typically higher plasma density and an average $\mathbf{B}_{GSE} = (25, -12, 66)$ nT.

The boundary layer can be separated into an inner region (09:21:24–10:07:30 UT) with variable, but overall stagnant flows $\mathbf{V}_{GSE} = (-8 \pm 48, 5 \pm 61, 3 \pm 32)$ km/s, plasma density $N = 6 \pm 3$ cm^{-3}, and $\mathbf{B}_{GSE} = (15 \pm 5, 6 \pm 8, 67 \pm 5)$ nT, and an outer region (10:07:30–11:27:40 UT) characterized by variable, magnetosheath-like flow $\mathbf{V}_{GSE} = (-161 \pm 56, 154 \pm 48, 50 \pm 33)$ km/s, and $N = 13 \pm 4$ cm^{-3}, which is dominated by many narrow CSs with a major By_{GSE} rotation of $\mathbf{B}_{GSE} = (15 \pm 9, 0 \pm 14, 73 \pm 7)$ nT, with values given as means and standard deviations. The MMS-SITL team made burst mode selections for the extended period 10:07:04–11:27:34 UT to allow further analysis of the sharp CS in this highly variable boundary layer region. The narrow CSs were almost exclusively encountered as MMS transitioned from a high-temperature boundary layer plasma of the magnetosphere into the cold magnetosheath as illustrated in Figure 1 (right) for a 20 min period of burst data. Two vertical dotted lines highlight the exhaust-related CS presented in this letter.

A power spectrum of the continuous T_{iAVG} burst observations (not shown) resulted in a dominant peak for all four MMS spacecraft at 15.8 mHz ($T = 63$ s). The nature of this periodic magnetopause surface wave that persists for at least 80 min can be explored using linear KH instability growth theory [*Chandrasekhar*, 1961]

$$\gamma^2 = \rho_1 \rho_2 / (\rho_1 + \rho_2)^2 [\mathbf{k} \cdot (\mathbf{U}_1 - \mathbf{U}_2)]^2 - \left[(\mathbf{k} \cdot \mathbf{B}_1)^2 + (\mathbf{k} \cdot \mathbf{B}_2)^2 \right] / \mu_0 (\rho_1 + \rho_2) \tag{1}$$

Equation (1) states the growth rate γ in terms of quantities evaluated in the magnetosphere (1) and magnetosheath (2) where μ_0 is the permeability of free space, ρ is the proton mass density, $\mathbf{B}$ is the magnetic field, $\mathbf{U}$ is the plasma flow velocity, and $\mathbf{k} = (k\cos\theta, 0, k\sin\theta)$ is the direction of wave propagation with amplitude $k = 2\pi/\lambda$ in a global boundary normal coordinate system (x,y,z). This system is defined such that $\mathbf{y}$ is the direction normal to the unperturbed magnetopause, $\mathbf{x}$ is positive toward the Sun along the magnetopause, and $\mathbf{z}$ completes the orthogonal system. Here θ is the angle between $\mathbf{k}$ and the xy plane of the flow shear. Equation (1) may be rearranged [*Nakamura et al.*, 2006] as
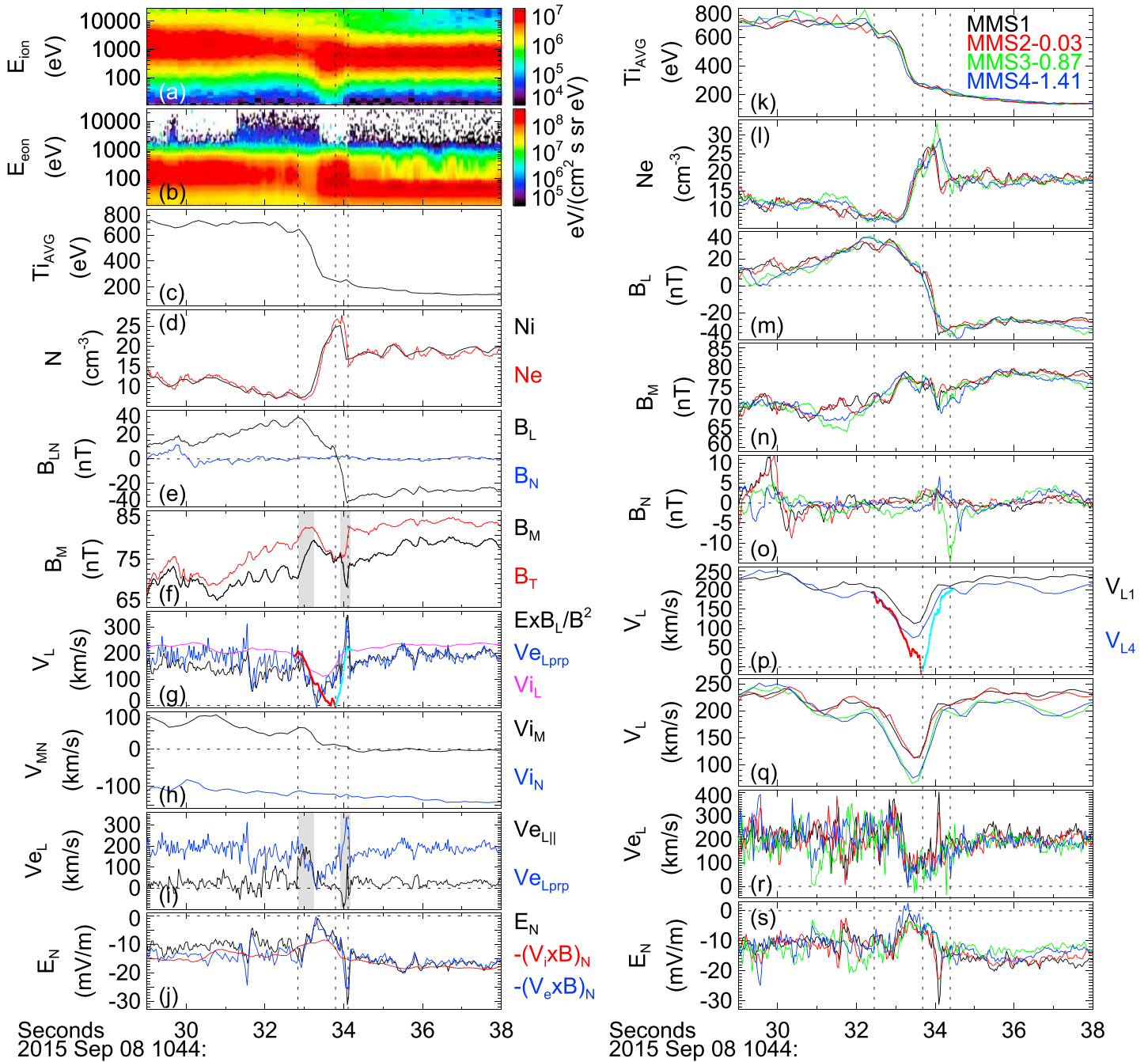
Figure 2. (a–j) MMS-1 burst observations in local boundary normal LMN coordinates at 10:44:29–10:44:38 UT on 8 September 2015. MMS-1 encountered a CS between 10:44:32.92 UT (first line) and 10:44:34.11 UT (third line). The panels show (a) ion and (b) electron energy-time spectrograms, (c) T_{iAVG}, (d) N_i (black) and N_e (red), (e) B_L (black) and B_N (blue), (f) B_M (black) and $|\mathbf{B}|$ (red), (g) perpendicular V_{eLperp} (blue), $(\mathbf{E} \times \mathbf{B})_L$ (black), V_{iL} (pink), and Walén predictions $V_{L1} = V_{L01} + \Delta V_{L1}$ (red) and $V_{L2} = V_{L02} + \Delta V_{L2}$ (cyan), (h) V_{iM} (black) and V_{iN} (blue), (i) L components of the perpendicular electron velocity (V_{eLperp}, blue) and parallel electron velocity ($V_{eL\parallel}$, black) with vertical bars indicating times of B_M gradients, and (j) measured electric field E_N (black), $-(\mathbf{V}_i \times \mathbf{B})_N$ (red), and $-(\mathbf{V}_e \times \mathbf{B})_N$ (blue). (k–s) Color-coded MMS burst observations with optimum time delays to MMS-1 shown in seconds. The panels show (k) T_{iAVG}, (l) N_e, (m) B_L, (n) B_M, (o) B_N, (p) observed V_{iL} at MMS-1 (black) and MMS-4 (blue) with Walén predictions using MMS-4, (q) V_{iL}, (r) V_{eL}, and (s) E_N. Vertical lines at 10:44:32.45 and 10:44:34.38 UT mark the MMS-4 CS. All components are shown using $\mathbf{L}_{GSE} = [-0.290, 0.956, -0.030]$, $\mathbf{M}_{GSE} = [0.224, 0.099, 0.970]$, and $\mathbf{N}_{GSE} = [0.930, 0.275, -0.243]$.

$$(\gamma/k)^2 = \rho_1\rho_2/(\rho_1 + \rho_2)^2(\Delta U_x \cos\theta + \Delta U_z \sin\theta)^2$$

$$-\left[(B_{1x}\cos\theta + B_{1z}\sin\theta)^2 + (B_{2x}\cos\theta + B_{2z}\sin\theta)^2\right]/\mu_0(\rho_1 + \rho_2) \tag{2}$$

and evaluated for the range of propagation angles that could result in a positive KH growth given the parameters measured on the two sides of the magnetopause. Five global boundary normal systems were examined, including a maximum flow shear system with $\mathbf{x} = -(\mathbf{U}_2 - \mathbf{U}_1)/|\mathbf{U}_2 - \mathbf{U}_1|$, a cross product normal system (cf. supporting information), and three standard systems [*Fairfield*, 1971; *Petrinec et al.*, 1991; *Roelof and Sibeck*, 1993]. We averaged MMS fast survey measurements of $\rho_1 = m_p N_1$, $\mathbf{B}_1$, and $\mathbf{U}_1$ from an inner boundary layer interval at 09:45:12–09:45:59 UT and magnetosheath measurements of $\rho_2 = m_p N_2$, $\mathbf{B}_2$, and $\mathbf{U}_2$ from a PDL-like interval at 11:27:40–11:28:40 UT (see Table S3 in the supporting information). The flow shear $\Delta\mathbf{U} = \mathbf{U}_1 - \mathbf{U}_2$ and $\mathbf{B}$ were such that all systems resulted in $(\gamma/k)^2 > 0$ for $\theta = \theta_0 \pm \Delta\theta$ with $\Delta\theta \sim 17°$ (see Figure S2 in the supporting information). A maximum wave growth $\gamma/k > 131$ km/s was obtained for a coordinate system-dependent angle θ_0 with $\gamma/k = 135$ km/s for the maximum shear system.

3. MMS Burst Mode Observations of Two Ion-Scale Current Sheets

A total of 42 CS (cf. supporting information) were analyzed for evidence of reconnection exhausts in a local LMN coordinate system as MMS transitioned from the boundary layer into the magnetosheath using burst data and the pressure anisotropy-weighted Walén relation based on tangential momentum balance [*Paschmann et al.*, 1986]. The boundary normal to each CS was estimated using MMS-1 observations and a local cross product normal $\mathbf{N} = \mathbf{B}_1 \times \mathbf{B}_2/|\mathbf{B}_1 \times \mathbf{B}_2|$ where $\mathbf{B}_1$ and $\mathbf{B}_2$ are the 2 s average magnetic fields on either side of the magnetopause CS. The guide-field $\mathbf{M}$ direction is defined as the unit vector of the cross product between $\mathbf{N}$ and the maximum variance direction of $\mathbf{B}$ [*Sonnerup and Scheible*, 1998] across the CS. $\mathbf{L} = \mathbf{M} \times \mathbf{N}$ completes the system. The Walén relation is stated as $V_L = V_{L0} + \Delta V_L$ where V_{L0} is the L component of the reference velocity on either side of the CS, $\Delta V_L(t) = \pm[B_L(1 - \alpha) - B_{L0}(1 - \alpha_0)]/[\rho_0\mu_0(1 - \alpha_0)]^{0.5}$, and $\alpha = (P_{||} - P_\perp)\mu_0/B^2$ between the parallel and perpendicular ion plasma pressures. The ΔV_L expression is applied separately from the two external sides (subscript 0) of a CS toward a joint center location due to the presence of similar plasma density and field strength across the CS. The choice of $\pm$ sign depends on whether B_L and V_L variations are in phase or not across the exhaust boundary. The remainder of this section is devoted to detailed observations recorded across two of the 22 CS with reconnection exhaust signatures. The mean directions of the three $\mathbf{L}$, $\mathbf{M}$, $\mathbf{N}$ unit vectors in these 22 cases are $\mathbf{N}_{GSE} = [0.92, 0.31, -0.22]$, $\mathbf{L}_{GSE} = [-0.34, 0.94, -0.10]$, and $\mathbf{M}_{GSE} = [0.13, 0.11, 0.99]$.

Figures 2a–2j show MMS-1 burst observations during a 9 s interval that straddles the boundary layer ($N_1 = 9$ cm^{-3}) and the magnetosheath ($N_2 = 18$ cm^{-3}) with an average $L_i = c/\omega_{pi} = 65$ km ion inertial length, where c is the speed of light and $\omega_{pi} = (N_0 e^2/m_p \varepsilon_0)^{1/2}$. A narrow 1.3 s wide CS is centered at 10:44:33.79 UT during which $\mathbf{B}$ displayed a rotation from $B_{L1} = 32$ nT to $B_{L2} = -34$ nT. The B_L rotation coincides with a weak but positive normal field $B_N = 1.3$ nT. MMS-1 measured a steady $V_{N0} = -122$ km/s and $V_{L0} = 217$ km/s external ion flow on either side of the CS, suggesting a mere 2.4 L_i normal width of the CS. A relatively weak and negative $\Delta V_{iL} = -100$ km/s ion jet was recorded across the CS relative to V_{L0}, which is ~110 km/s slower than the jet speed predicted by the Walén relation and the speed observed by $(\mathbf{E} \times \mathbf{B})_L$ and the L component of the perpendicular electron velocity, V_{eLperp}. The out-of-plane B_M field experienced an asymmetric, bipolar perturbation that consisted of a wide $\Delta B_M = 7.8$ nT increase relative to $B_{M1} = 71$ nT on the magnetospheric side followed by a 23 km wide sub-ion scale (190 ms duration) $\Delta B_M = -4.4$ nT depression relative to $B_{M2} = 74$ nT on the magnetosheath side. The B_M depression coincides with a fast $V_{eLperp} > 0$ and a normal electric field $E_N = -31$ mV/m. This $\Delta E_N = -19$ mV/m electric field relative to a background $E_{N2} = -13$ mV/m was recorded by the electron $-\mathbf{V}_e \times \mathbf{B}$ electric field but not by the ion $-\mathbf{V}_i \times \mathbf{B}$. The bipolar ΔB_M signature is in qualitative agreement with an asymmetric Hall $\mathbf{B}$ supported by in-plane Hall electron currents in this strong $B_M/B_L = 2.2$ guide-field. Figure 2i indicates where the in-plane projection of the field-aligned electron velocity ($V_{eL||}$) helps support the three individual B_M gradients [*Eriksson et al.*, 2015]. The asymmetric $\Delta E_N < 0$ electric field is consistent with a highly localized Hall electric field [cf. *Drake et al.*, 2009, Figure 1c)] on the magnetosheath side.

Figures 2k–2s compare these MMS-1 measurements with those recorded by the neighboring MMS spacecraft with appropriate time delays. MMS-2, separated by $[\Delta s_L, \Delta s_M, \Delta s_N] = [10.5, -153.6, -5.1]$ km from MMS-1 and by 0.03 s in time, recorded nearly identical signatures as MMS-1 including an enhanced $\Delta E_N < 0$ of
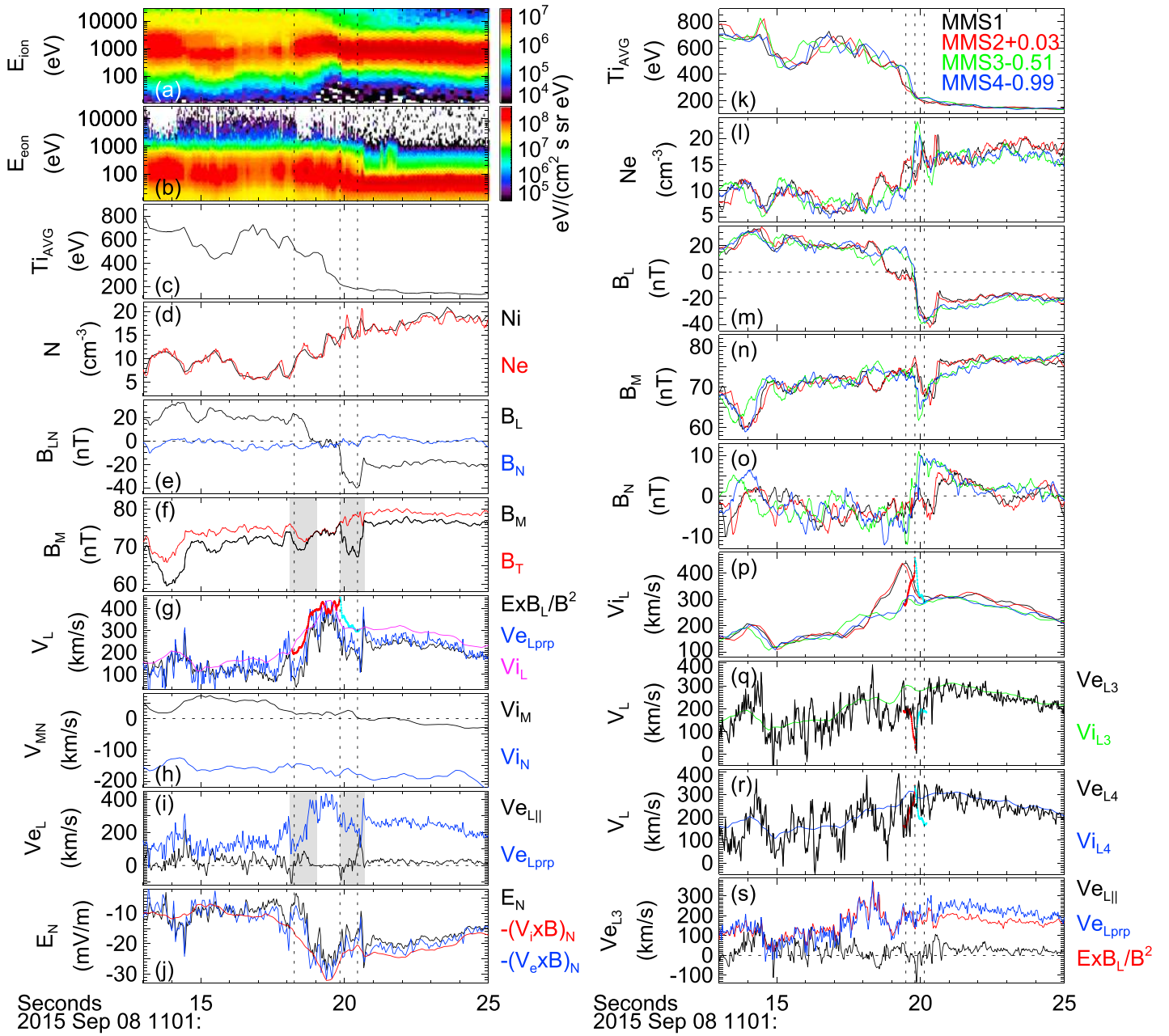
Figure 3. (a–j) MMS-1 burst observations in local LMN at 11:01:13–11:01:25 UT on 8 September 2015 (cf. Figure 2). First and last vertical dotted lines at 11:01:18.25 and 11:01:20.45 UT mark the MMS-1 CS. (k–s) Color-coded MMS burst observations for optimum time delays relative to MMS-1. Same panels as Figure 2 except V_{iL} for all spacecraft and Walén prediction at MMS-4 (Figure 3p), V_{eL} and V_{iL} at MMS-3 with negative Walén jet prediction at MMS-3 (Figure 3q), V_{eL} and V_{iL} at MMS-4 with positive Walén jet prediction at MMS-4 (Figure 3r), and MMS-3 comparison of V_{eL} and $\mathbf{E} \times \mathbf{B}_L$ (Figure 3s). Vertical lines mark the MMS-4 CS at 11:01:19.49–11:01:20.13 UT. All components are shown using $\mathbf{L}_{GSE} = [-0.171, 0.984, -0.057]$, $\mathbf{M}_{GSE} = [0.253, 0.100, 0.962]$, and $\mathbf{N}_{GSE} = [0.952, 0.150, -0.266]$.

weaker magnitude toward the magnetosheath side of the exhaust. These similarities and the ~2.4 L_i separation along the guide-field suggest a roughly two-dimensional exhaust over the MMS tetrahedron. The MMS-3,4 pair observed important differences from the MMS-1,2 pair. This includes a wider 3.6 L_i exhaust as indicated by V_{iL} and B_L over $\Delta t = 1.9$ s. They also observed a wider ΔB_M depression and a faster $\Delta V_{iL} = -125$ km/s jet, but no Hall-related $\Delta E_N < 0$. MMS-3 was separated by $\Delta t_{13} = 0.87$ s in time and $[\Delta s_L, \Delta s_M, \Delta s_N] = [-127.4, -77.4, -86.5]$ km from MMS-1. MMS-4 was separated by $\Delta t_{14} = 1.41$ s and $[\Delta s_L, \Delta s_M, \Delta s_N] = [59.1, -86.3, -149.3]$ km from MMS-1. The deHoffmann-Teller (HT) velocity [*Khrabrov and*
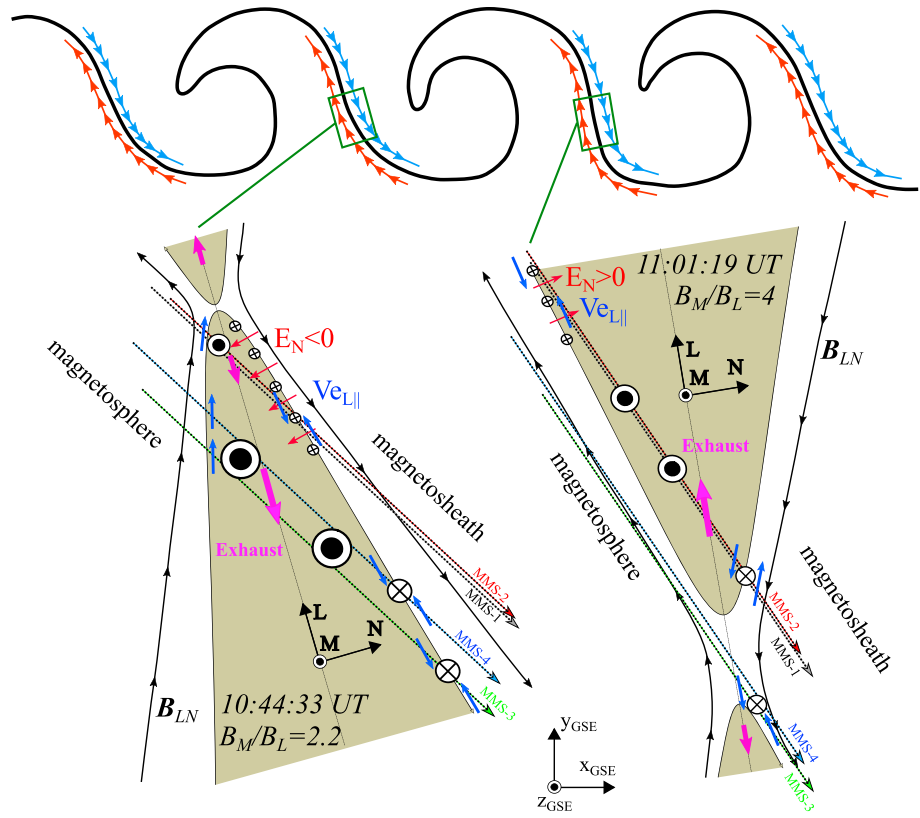
Figure 4. Illustration of the **NL**-plane orientation of two KH-related trailing CSs centered at (bottom, left) ~10:44:33 UT and (bottom, right) ~11:01:19 UT with $\mathbf{x}_{GSE}$ to the right. Color-coded MMS trajectories are shown across two ion exhaust regions (shaded). Asymmetric Hall B_M fields are shown with field depressions ($\Delta B_M < 0$) as encircled crosses, and field enhancements ($\Delta B_M > 0$) as encircled dots. Hall ΔE_N fields are shown as red arrows. In-plane projections of the field-aligned electron velocity ($V_{eL||}$) are shown as blue arrows. The top schematic indicates the general location of these magnetopause CSs on a KH wave train from $B_L > 0$ (red arrows, boundary layer) to $B_L < 0$ (blue arrows, magnetosheath). The actual observations were separated by several KH-related CSs.

Sonnerup, 1998] across the CS at MMS-1, $\mathbf{V}_{HT} = [V_{HTL}, V_{HTM}, V_{HTN}] = [174, 70, -122]$ km/s, suggests that additional corrections $V_{HTL}\Delta t$ in the negative **L** direction due to X line drift in the positive **L** direction, and their time delays would put MMS-3,4 roughly 3–4 L_i along the exhaust from MMS-1,2. The MMS-1,2 pair was thus closer to the X line than the MMS-3,4 pair which explains a slower ion exhaust and the presence of asymmetric Hall electric fields.

Figure 3 (a–j) presents a narrow 2.2 s wide and highly bifurcated CS without a clear density enhancement at 11:01:19.84 UT as MMS-1 transitioned from a boundary layer ($N_1 = 7$ cm^{-3}, $B_{L1} = 18$ nT, $B_{M1} = 72$ nT) into the magnetosheath ($N_2 = 17$ cm^{-3}, $B_{L2} = -20$ nT, $B_{M2} = 76$ nT) with an average $L_i = 72$ km. A fast positive exhaust was present in V_{iL}, V_{eLperp}, and $(\mathbf{E} \times \mathbf{B})_L/B^2$ at the CS with V_{iL} in agreement with the Walén prediction. **B** was dominated by the guide-field within this 5.3 L_i wide exhaust where $B_L = -1.4$ nT, while $B_N = -3.3$ nT is consistent with an exhaust in the positive **L** direction. The magnetosheath side was characterized by an additional $\Delta B_L = 18$ nT compression of the adjacent background $B_{L2} = -20$ nT that coincided with a guide-field $\Delta B_M = -9$ nT depression relative to the external guide-field $B_{M2} = 76$ nT. This $\Delta B_M < 0$ is not consistent with a Hall field on the magnetosheath side of a positive L exhaust from a single X line, and there is only a weak Hall-like $\Delta B_M = -3$ nT depression signature on the earthward side of the exhaust. The measured E_N suggests a broad, $\Delta E_N > 0$ electric field relative to $-(\mathbf{V}_i \times \mathbf{B})_N$ during the weak ΔB_M depression. $\Delta E_N > 0$ is consistent with $-(\mathbf{V}_e \times \mathbf{B})_N$, confirming $\Delta B_M = -3$ nT and $\Delta E_N > 0$ as a weak Hall **B** and **E**. Figure 3i suggests that $V_{eL||}$ is qualitatively consistent with in-plane electron currents to support the individual B_M gradients of the weak Hall ΔB_M depression and the stronger $\Delta B_M = -9$ nT on the magnetosheath side.

Figure 3 (k–s) shows the corresponding observations from the other spacecraft. MMS-2 again observed nearly identical exhaust signatures as MMS-1 across this CS with a relative separation vector

$[\Delta s_L, \Delta s_M, \Delta s_N] = [10.8, -155.7, 0.0]$ km from MMS-1. MMS-3 and MMS-4, delayed by $\Delta t_{13} = 0.51$ s and $\Delta t_{14} = 0.99$ s from MMS-1, did not observe an ion exhaust across the CS (Figure 3p), although they both recorded a density enhancement. The absence of an ion exhaust is apparently related to the short 0.64 s duration of this CS at MMS-4 with a ~110 km (1.5 L_i) normal width. MMS-3 and MMS-4 were 3.9 L_i and 3.6 L_i closer to the X line, respectively, than MMS-1 based on $\mathbf{V}_{HT} = [V_{HTL}, V_{HTM}, V_{HTN}] = [304, 104, -169]$ km/s and their initial separations $\Delta s_L = -128$ km (MMS-3) and $\Delta s_L = 44$ km (MMS-4) from MMS-1. MMS-3 observed a narrow, positive V_{eL} electron jet (Figure 3q) on the $B_N < 0$ side (Figure 3o) of the CS followed by a narrow, negative V_{eL} jet on the $B_N > 0$ side of the CS, consistent with a Walén jet prediction. MMS-4 observed a more variable V_{eL} (Figure 3r) than MMS-3 across the CS. However, there was no evidence of a negative V_{eL} jet. The Walén relation rather indicates that MMS-4 may have observed a positive V_{eL} jet on the $B_N < 0$ side. These observations suggest a scenario where MMS-3 and MMS-4 transitioned near an electron diffusion region (EDR) along the negative **L** direction in a strong $B_M/B_L = 4$ guide-field.

Figure 4 summarizes the MMS observations of Figures 2 and 3. MMS trajectories are based on the in-plane $\mathbf{V}_{HT}$ across each CS, while L separations are based on the tetrahedron, time delays, and V_{HTL}. MMS-2 is projected onto the NL plane with a larger separation from MMS-1 for clarity. Figure 4 emphasizes along-track observations of exhausts (shaded), ΔB_M variations (circles) relative to the guide-field, $V_{eL\parallel}$ (blue arrows), and $E_N = -(\mathbf{V}_e \times \mathbf{B})_N$ relative to $-(\mathbf{V}_i \times \mathbf{B})_N$ (red arrows). $V_{eL\parallel}$ is in qualitative agreement with in-plane currents to support the B_M gradients [*Eriksson et al.*, 2015]. The strong guide-field induces the observed Hall **B** asymmetry with narrow ΔB_M depressions shunted away from the CS toward the exhaust boundary [*Eastwood et al.*, 2010] with a similar response of the normal ΔE_N [*Drake et al.*, 2009; *Eastwood et al.*, 2010]. It is unclear why MMS-3 and MMS-4 did not observe $\Delta E_N < 0$ across the magnetosheath side of the exhaust boundary at ~10:44:35 UT. The wide $\Delta E_N > 0$ observed by MMS-1 across the earthward side of the exhaust at ~11:01:18.5 UT is consistent with a trajectory skimming the exhaust boundary due to motion of the structure along the **L** direction. Finally, it is unclear why a strong $\Delta B_M < 0$ depression exists on the magnetosheath side of the exhaust at ~11:01:20 UT. However, in-plane currents due to $V_{eL\parallel}$ qualitatively agree with this $\Delta B_M < 0$ that may be related to similar guide-field effects reported by *Eriksson et al.* [2015, 2016].

4. Summary and Conclusions

We have reported the first direct evidence of magnetic reconnection exhausts in the equatorial xy_{GSE} plane and asymmetric Hall **B** and **E** associated with Kelvin-Helmholtz waves and a strong guide-field along the duskside magnetopause on 8 September 2015. The analysis was focused on 42 sunward facing, ion-scale CS between a preexisting, low-latitude boundary layer and the magnetosheath as observed by MMS at 150–185 km spacecraft separation. The pressure anisotropy-weighted Walén relation confirmed ion exhausts at 22 of the 42 CS. The exhausts were immersed in a weakly asymmetric plasma density ratio, $1.25 < N_2/N_1 < 2.67$, between the adjacent magnetosheath and boundary layer sides of the CS. This is not expected to greatly affect Hall fields on the low-density side of the magnetopause CS [e.g., *Birn et al.*, 2008; *Pritchett*, 2008]. More importantly, there was a very strong external guide-field, with an average $\theta = 27° \pm 7°$ magnetic field shear angle across the local magnetopause corresponding to a large $B_M/B_L = 4.2$ between the guide-field and the reconnecting field. This is expected to cause strong Hall **B** and **E** asymmetries [e.g., *Drake et al.*, 2009; *Eastwood et al.*, 2010] as observed by MMS.

The 42 CS swept across the MMS formation at a locally measured in-plane ion speed $V_{NL} = 258 \pm 35$ km/s (cf. supporting information; $V_{N0} = -102 \pm 53$ km/s and $V_{L0} = 229 \pm 47$ km/s), in general agreement with the in-plane $\mathbf{V}_{HT}$ velocity, resulting in an estimated $\lambda_{KH} = 2.56 \pm 0.3 R_E$ KH wave period for $T_{KH} = 63.3$ s. A small $A_0 = 123$ km amplitude perturbation at 14.5 MLT would, e.g., grow to $A = A_0 e^{\gamma t} = \lambda_{KH}/2$ at MMS for $V_{KH} = 258$ km/s and $\gamma/k = 135$ km/s, where $\gamma \sim 0.052$ s^{-1}.

The 3.1 ± 1.8 s time durations of the 22 exhaust-related CS, with the most compressed CS sweeping by MMS-1 in only 1.2 s, correspond to $4.4 \pm 1.9 L_i$ normal widths (278 km) or $<2\%$ of λ_{KH} between consecutive CS. Exhausts were observed in a positive (outward) **L** direction in 9 cases and in a negative (inward) **L** direction in 13 cases along the local magnetopause CS. Most exhausts were observed in the same direction at all four MMS spacecraft, while showing intriguing spatial differences in V_{iL} exhaust speed. This is possibly related to relative distances from the X line consistent with local $|V_{eLperp} - V_{iL}|$ exhaust differences. One notable

exception was the wide exhaust encountered by the MMS-1,2 pair at 11:01:19 UT, when MMS-3 and MMS-4 observed a much narrower 1.5 L_i wide CS without ion exhausts. A pair of opposite V_{eL} electron jets at MMS-3, no $(\mathbf{E} \times \mathbf{B})_L/B^2$ exhaust, and a B_N rotation across the B_L gradient suggest that MMS-3 and MMS-4 traversed this CS in the vicinity of an EDR in a strong $B_M/B_L = 4$ guide-field.

MMS-1 and MMS-2 were separated along the guide-field **M** direction by 152 ± 4 km. They observed nearly identical field and plasma signatures, which confirm that the exhausts were locally 2-D on the scale of the MMS tetrahedron. MMS-3 and MMS-4 generally observed different field and plasma signatures from the MMS-1,2 pair due to separations from MMS-1 along the **L** direction.

These unprecedented high-resolution MMS observations are consistent with KH-associated magnetic reconnection at the sunward facing compressed CS of KH waves [e.g., *Hasegawa et al.*, 2009; *Nakamura et al.*, 2013], which allows for local transport of mass and energy across the flank magnetopause despite a large guide-field.

References

Birn, J., J. E. Borovsky, and M. Hesse (2008), Properties of asymmetric magnetic reconnection, *Phys. Plasmas*, *15*, 032101-1, doi:10.1063/1.2888491.

Burch, J. L., T. E. Moore, R. B. Torbert, and B. L. Giles (2015), Magnetospheric Multiscale overview and science objectives, *Space Sci. Rev.*, doi:10.1007/s11214-015-0164-9.

Chandrasekhar, S. (1961), *Hydrodynamic and Hydromagnetic Stability*, Oxford Univ. Press, New York.

Drake, J. F., P. A. Cassak, M. A. Shay, M. Swisdak, and E. Quataert (2009), A magnetic reconnection mechanism for ion acceleration and abundance enhancements in impulsive flares, *Astrophys. J.*, *700*, L16–L20, doi:10.1088/0004-637X/700/1/L16.

Eastwood, J. P., M. A. Shay, T. D. Phan, and M. Øieroset (2010), Asymmetry of the ion diffusion region Hall electric and magnetic fields during guide field reconnection: Observations and comparison with simulations, *Phys. Rev. Lett.*, *104*, doi:10.1103/PhysRevLett.104.205001.

Ergun, R. E., et al. (2014), The axial double probe and fields signal processing for the MMS mission, *Space Sci. Rev.*, doi:10.1007/s11214-014-0115-x.

Eriksson, S., G. Lapenta, D. L. Newman, T. D. Phan, J. T. Gosling, B. Lavraud, Y. V. Khotyaintsev, C. M. Carr, S. Markidis, and M. V. Goldman (2015), On multiple reconnection X-lines and tripolar perturbations of strong guide magnetic fields, *Astrophys. J.*, *805*, 43, doi:10.1088/0004-637X/805/1/43.

Eriksson, S., P. A. Cassak, A. Retinò, and F. S. Mozer (2016), Subsolar magnetopause observation and kinetic simulation of a tripolar guide magnetic field perturbation consistent with a magnetic island, *Geophys. Res. Lett.*, *43*, 3035–3041, doi:10.1002/2016GL068691.

Fairfield, D. H. (1971), Average and unusual locations of the Earth's magnetopause and bow shock, *J. Geophys. Res.*, *76*, 6700–6716, doi:10.1029/JA076i028p06700.

Fairfield, D. H., A. Otto, T. Mukai, S. Kokubun, R. P. Lepping, J. T. Steinberg, A. J. Lazarus, and T. Yamamoto (2000), Geotail observations of Kelvin-Helmholtz instability at the equatorial magnetotail boundary for parallel northward fields, *J. Geophys. Res.*, *105*, 21,159–21,174, doi:10.1029/1999JA000316.

Foullon, C., C. J. Farrugia, A. N. Fazakerley, C. J. Owen, F. T. Gratton, and R. B. Torbert (2008), Evolution of Kelvin-Helmholtz activity on the dusk flank magnetopause, *J. Geophys. Res.*, *113*, A11203, doi:10.1029/2008JA013175.

Fuselier, S. A., et al. (2014), Magnetospheric multiscale science mission profile and operations, *Space Sci. Rev.*, doi:10.1007/s11214-014-0087-x.

Hasegawa, H., M. Fujimoto, T.-D. Phan, H. Rème, A. Balogh, M. W. Dunlop, C. Hashimoto, and R. TanDoKoro (2004), Transport of solar wind into Earth's magnetosphere through rolled-up Kelvin-Helmholtz vortices, *Nature*, *430*, 755, doi:10.1038/nature02799.

Hasegawa, H., M. Fujimoto, K. Takagi, Y. Saito, T. Mukai, and H. Rème (2006), Single-spacecraft detection of rolled-up Kelvin-Helmholtz vortices at the flank magnetopause, *J. Geophys. Res.*, *111*, A09203, doi:10.1029/2006JA011728.

Hasegawa, H., et al. (2009), Kelvin-Helmholtz waves at the Earth's magnetopause: Multiscale development and associated reconnection, *J. Geophys. Res.*, *114*, A12207, doi:10.1029/2009JA014042.

Khrabrov, A. V., and B. U. Ö. Sonnerup (1998), DeHoffmann-Teller analysis, in *Analysis Methods for Multi-Spacecraft Data*, *ISSI Sci. Rep. SR-001*, edited by G. Paschmann and P. W. Daly, pp. 221–248, Eur. Space Agency Publ. Div, Noordwijk, Netherlands.

Kivelson, M. G., and S.-H. Chen (1995), The magnetopause: Surface waves and instabilities and their possible dynamic consequences, in *Physics of the Magnetopause*, *Geophys. Monogr. Ser*, vol. 90, edited by P. Song, B. U. Ö. Sonnerup, and M. F. Thomsen, pp. 257–268, AGU, Washington, D. C.

Knoll, D. A., and L. Chacón (2002), Magnetic reconnection in the two dimensional Kelvin-Helmholtz instability, *Phys. Rev. Lett.*, *88*(21), 215003.

Kokubun, S., H. Kawano, M. Nakamura, T. Yamamoto, K. Tsuruda, H. Hayakawa, A. Matsuoka, and L. A. Frank (1994), Quasi-periodic oscillations of the magnetopause during northward sheath magnetic field, *Geophys. Res. Lett.*, *21*(25), 2883–2886, doi:10.1029/94GL02103.

Lindqvist, P.-A., et al. (2014), The spin-plane double probe electric field instrument for MMS, *Space Sci. Rev.*, doi:10.1007/s11214-014-0116-9.

Miura, A., and P. L. Pritchett (1982), Nonlocal stability analysis of the MHD Kelvin-Helmholtz instability in a compressible plasma, *J. Geophys. Res.*, *87*, 7431–7444, doi:10.1029/JA087iA09p07431.

Nakamura, T. K. M., and M. Fujimoto (2005), Magnetic reconnection within rolled-up MHD-scale Kelvin-Helmholtz vortices: Two-fluid simulations including finite electron inertial effects, *Geophys. Res. Lett.*, *32*, L21102, doi:10.1029/2005GL023362.

Nakamura, T. K. M., M. Fujimoto, and A. Otto (2006), Magnetic reconnection induced by weak Kelvin-Helmholtz instability and the formation of the low-latitude boundary layer, *Geophys. Res. Lett.*, *33*, L14106, doi:10.1029/2006GL026318.

Nakamura, T. K. M., M. Fujimoto, and A. Otto (2008), Structure of an MHD-scale Kelvin-Helmholtz vortex: Two-dimensional two-fluid simulations including finite electron inertial effects, *J. Geophys. Res.*, *113*, A09204, doi:10.1029/2007JA012803.

Nakamura, T. K. M., W. Daughton, H. Karimabadi, and S. Eriksson (2013), Three-dimensional dynamics of vortex-induced reconnection and comparison with THEMIS observations, *J. Geophys. Res. Space Physics*, *118*, 5742–5757, doi:10.1002/jgra.50547.

Nykyri, K., and A. Otto (2001), Plasma transport at the magnetospheric boundary due to reconnection in Kelvin-Helmholtz vortices, *Geophys. Res. Lett.*, *28*, 3565–3568, doi:10.1029/2001GL013239.

Nykyri, K., A. Otto, B. Lavraud, C. Mouikis, L. M. Kistler, A. Balogh, and H. Rème (2006), Cluster observations of reconnection due to the Kelvin-Helmholtz instability at the dawnside magnetospheric flank, *Ann. Geophys.*, *24*, 2619.

Paschmann, G., I. Papamastorakis, W. Baumjohann, N. Sckopke, C. W. Carlson, B. U. Ö. Sonnerup, and H. Luhr (1986), The magnetopause for large magnetic shear: AMPTE/IRM observations, *J. Geophys. Res.*, *91*, 11,099–11,115, doi:10.1029/JA091iA10p11099.

Petrinec, S. P., P. Song, and C. T. Russell (1991), Solar cycle variations in the size and shape of the magnetopause, *J. Geophys. Res.*, *96*, 7893–7896, doi:10.1029/90JA02566.

Pollock, C. J., et al. (2016), Fast plasma investigation for Magnetospheric Multiscale, *Space Sci. Rev.*, doi:10.1007/s11214-016-0245-4.

Pritchett, P. L. (2001), Geospace environment modeling magnetic reconnection challenge: Simulations with a full particle electromagnetic code, *J. Geophys. Res.*, *106*, 3783–3798, doi:10.1029/1999JA001006.

Pritchett, P. L. (2008), Collisionless magnetic reconnection in an asymmetric current sheet, *J. Geophys. Res.*, *113*, A06210, doi:10.1029/2007JA012930.

Pu, Z. Y., M. Yan, and Z. X. Liu (1990), Generation of vortex induced-tearing mode instability at the magnetopause, *J. Geophys. Res.*, *95*, 10559, doi:10.1029/JA095iA07p10559.

Roelof, E. C., and D. G. Sibeck (1993), Magnetopause shape as a bivariate function of interplanetary magnetic field Bz and solar wind dynamic pressure, *J. Geophys. Res.*, *98*, 21,421–21,450, doi:10.1029/93JA02362.

Russell, C. T., et al. (2014), The Magnetospheric Multiscale magnetometers, *Space Sci. Rev.*, doi:10.1007/s11214-014-0057-3.

Sonnerup, B. U. Ö. (1979), Magnetic field reconnection, in *Solar System Plasma Physics*, edited by L. J. Lanzerotti, C. Kennel, and E. Parker, pp. 47–108, North-Holland, Amsterdam.

Sonnerup, B. U. Ö., and M. Scheible (1998), Minimum and maximum variance analysis, in *Analysis Methods for Multi-Spacecraft Data*, *ISSI Sci. Rep. SR-001*, edited by G. Paschmann and P. W. Daly, pp. 185–220, Eur. Space Agency Publ. Div, Noordwijk, Netherlands.

Terasawa, T. (1983), Hall current effect on tearing mode instability, *Geophys. Res. Lett.*, *10*, 475–478, doi:10.1029/GL010i006p00475.

Torbert, R. B., et al. (2014), The FIELDS instrument suite on MMS: Scientific objectives, measurements, and data products, *Space Sci. Rev.*, doi:10.1007/s11214-014-0109-8.

Wang, Y. L., J. Raeder, C. T. Russell, T. D. Phan, and M. Manapat (2003), Plasma depletion layer: Event studies with a global model, *J. Geophys. Res.*, *108*(A1), 1010, doi:10.1029/2002JA009281.